Supplementary Information

Antiferromagnetic Fe_3As nanostructure with a unique planar Fe arrangement

cXu Yan[1,†], Fanjunjie Han[2,†], Yong Liu[1], and Guochun Yang[1,2,3*]

[1]*State Key Laboratory of Metastable Materials Science & Technology and Key Laboratory for Microstructural Material Physics of Hebei Province, School of Science, Yanshan University, Qinhuangdao 066004, China*

[2]*Centre for Advanced Optoelectronic Functional Materials Research and Key Laboratory for UV Light-Emitting Materials and Technology of Northeast Normal University, Changchun 130024, China*

[3]*Key Laboratory of Functional Materials Physics and Chemistry of the Ministry of Education, College of Physics, and National Demonstration Center for Experimental Physics Education, Jilin Normal University, Changchun 130103, P. R. China*

Index **page**

Computational Details

The particle swarm optimization (PSO) method within the evolutionary algorithm as implemented in the Crystal structure Analysis by Particle Swarm Optimization (CALYPSO) code[1,2] was employed to find the lowest energy structures of Fe_xAs (x = 3 and 4) monolayers. Unit cells containing 2 and 4 formula units (f.u.) with buckled and planar structures were considered. In the first step, random structures with certain symmetry were constructed in which atomic coordinates were generated by the crystallographic symmetry operations. Local optimizations using the VASP code[3] were done with the conjugate gradients method and stopped when Gibbs free energy changes became smaller than 1×10^{-6} eV per cell. After processing the first-generation structures, 60% of them with lower enthalpies were selected to construct the next generation structures by Particle Swarm Optimization (PSO). 40% of the structures in the new generation were randomly generated. A structure fingerprinting technique of bond characterization matrix was applied to the generated structures, so that identical structures were strictly forbidden. These procedures significantly enhance the diversity of the structures, which is crucial for structural global search efficiency. In most cases, structural searching simulations for each calculation were stopped after generating 1000 ~ 1200 structures (e.g., about 20 ~ 30 generations). The local structural relaxations and electronic properties calculations were performed in the framework of the density functional theory (DFT)[4] within the generalized gradient approximation (GGA)[5] as implemented in the VASP code. The $3d^7 4s^1$ and $4s^2 4p^3$ atomic orbitals were treated as valence states for Fe and As, respectively. The cut-off energy for the expansion of wavefunctions into plane waves was set to 450 eV in calculations. Phonon calculations were performed for a $3 \times 3 \times 1$ supercell for Fe_3As by using a supercell approach with the finite displacement method[6] as implemented in the PHONOPY code.[7] First-principles molecular dynamics (MD) simulations[8] for a $4 \times 4 \times 1$ Fe_3As supercell were performed in NVT ensemble lasted for 6 ps with a time step of 1 fs at 500 K. The temperature was controlled by using the Nosé-Hoover method. The Monte Carlo simulations based on the Ising model were performed using the MCSOLVER package.[9] The VASPKIT code[10] were used for pre- and post-processing calculations.

Mechanical stability

The strain was defined as, $\varepsilon = \frac{a - a_0}{a_0} \times 100\% = \frac{b - b_0}{b_0} \times 100\%$, where a, b and a_0, b_0 are the lattice constants of the unit cell under strain and at equilibrium, respectively. Positive and negative value match to biaxial tensile and compressive strain, separately.

To further verify the mechanical stability of the Fe_3As monolayer, we calculated its elastic constants[11,12]. Based on Born criteria[13], the elastic constant constitutes a symmetric 6 × 6 tensor matrix in the linear elastic range. The elastic constants were calculated to be C_{11} = 102.362 N/m, C_{22} = 98.088 N/m, C_{12} = 35.157 N/m, and C_{66} = 29.612 N/m. C_{11}, $C_{66} > 0$ and $C_{11}C_{22} - C_{12}^2 > 0$, confirming the Fe_3As monolayer is mechanically stable. The mechanical performance was explored by the in-plane Young's modulus $Y(\theta)$ and Poisson's ratio $v(\theta)$ as follows

$$Y(\theta) = \frac{C_{11}C_{22} - C_{12}^2}{C_{11}s^4 + C_{22}c^4 + As^2c^2}$$

$$v(\theta) = \frac{Bc^2s^2 - C_{12}(c^4 + s^4)}{C_{11}s^4 + C_{22}c^4 + As^2c^2}$$

where

$$s = sin\theta$$

$$c = cos\theta$$

$$A = (C_{11}C_{22} - C_{12}^2)/C_{66} - 2C_{12}$$

$$B = C_{11} + C_{22} - (C_{11}C_{22} - C_{12}^2)/C_{66}$$

Cohesive energy calculation

We used the following formula to calculate the cohesive energy per atom

$$E_{coh} = \frac{3E_{Fe} + E_{As} - E_{Fe_3As}}{4}$$

where E_{Fe}, E_{As}, and E_{Fe_3As} are the energies of the Fe, As atom, and Fe_3As unit cell, respectively.

Magnetic coupling parameters calculation

Here, the effective spin Hamiltonian was defined as

$$\hat{H} = \sum_{ij} J_1 \vec{S}_i \vec{S}_j + \sum_{jk} J_2 \vec{S}_j \vec{S}_k + \sum_{jm} J_3 \vec{S}_j \vec{S}_m + \sum_{kk} J_4 \vec{S}_k \vec{S}_k + \sum_{jj} J_5 \vec{S}_j \vec{S}_j + \sum_{km} J_6 \vec{S}_k + E_0$$

where *J*s represent the magnetic coupling interaction parament between adjacent Fe atoms, *S* is the spin of Fe atom, value as 3/2 here. In order to get the value of *J*s, we considered the energy nine configurations in a 2 × 2 × 1 supercell with the following:

$$E_{\mathrm{FM}} = -4J_1S^2 - 16J_2S^2 - 4J_3S^2 - 4J_4S^2 - 8J_5S^2 - 16J_6S^2 - 8J_7S^2 - 4J_8S^2 + E_0$$

$$E_{\mathrm{AFM1}} = -4J_1S^2 - 16J_2S^2 + 4J_3S^2 - 4J_4S^2 - 8J_5S^2 + 16J_6S^2 + 8J_7S^2 + 4J_8S^2 + E_0$$

$$E_{\mathrm{AFM2}} = 4J_1S^2 + 4J_3S^2 - 4J_4S^2 - 8J_5S^2 - 16J_6S^2 + 8J_7S^2 + 4J_8S^2 + E_0$$

$$E_{\mathrm{AFM3}} = -4J_1S^2 - 4J_3S^2 + 4J_4S^2 + 8J_5S^2 + 8J_7S^2 - 4J_8S^2 + E_0$$

$$E_{\mathrm{AFM4}} = -4J_1S^2 + 4J_3S^2 + 4J_4S^2 + 8J_5S^2 - 8J_7S^2 + 4J_8S^2 + E_0$$

$$E_{\mathrm{AFM5}} = -4J_1S^2 - 4J_3S^2 + 4J_4S^2 + 8J_5S^2 + 8J_7S^2 + 4J_8S^2 + E_0$$

$$E_{\mathrm{AFM6}} = -4J_1S^2 + 4J_3S^2 + 4J_4S^2 + 8J_5S^2 - 8J_7S^2 - 4J_8S^2 + E_0$$

$$E_{\mathrm{FIM2}} = 4J_1S^2 + 4J_3S^2 - 4J_4S^2 - 8J_5S^2 + 8J_7S^2 - 4J_8S^2 + E_0$$

$$E_{\mathrm{FIM3}} = -4J_1S^2 - 4J_3S^2 - 4J_4S^2 + 8J_5S^2 + 8J_7S^2 - 4J_8S^2 + E_0$$

Supplementary Figures

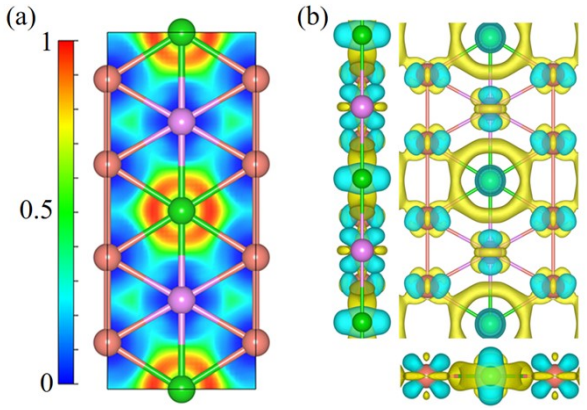

Fig. S1 (a) Electron localization function (ELF) and (b) difference charge density of the Fe_3As monolayer, in which cyan and yellow areas represent electron gains and losses, respectively.

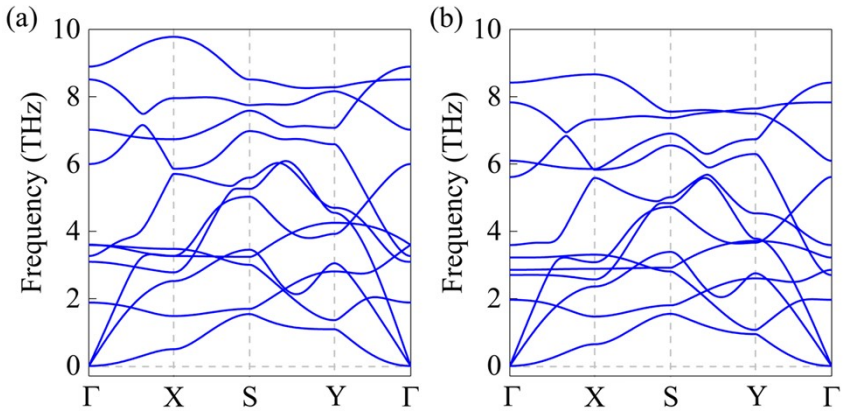

Fig. S2 Phonon dispersion curves of the Fe_3As monolayer at (a) 300 and (b) 500 K, respectively.

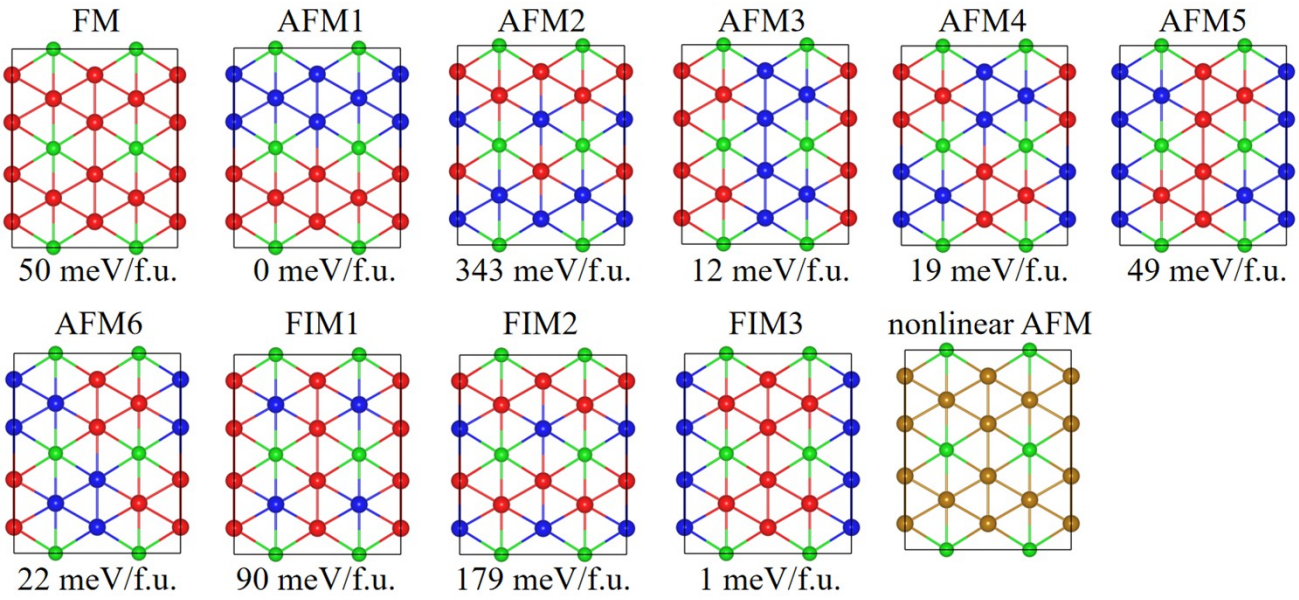

Fig. S3 Eleven different magnetic configurations of the Fe_3As monolayer and their corresponding energies. The red and blue balls represent spin-up and spin-down Fe atoms, respectively.

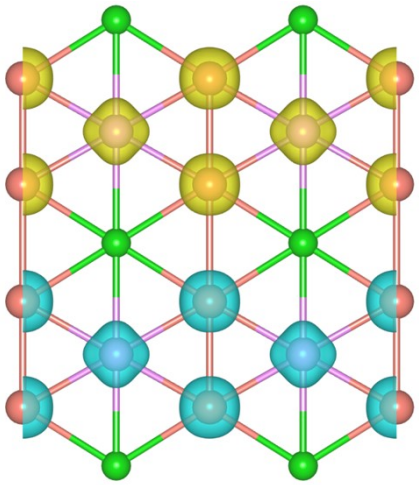

Fig. S4 Spin charge density of the Fe_3As monolayer, in which the blue and yellow isosurfaces represent different spin states.

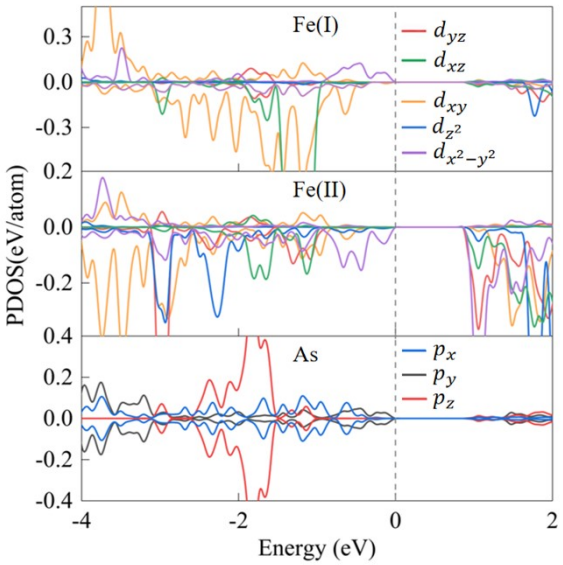

Fig. S5 Partial density of states (PDOS) of Fe and As atoms in the Fe_3As monolayer. The Fermi level is set to zero.

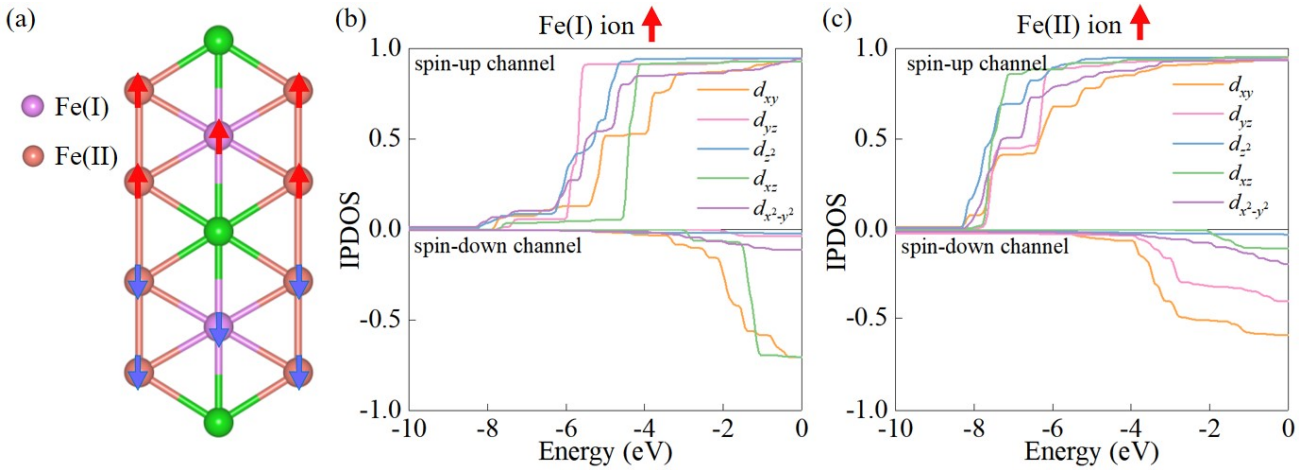

Fig. S6 (a) Magnetic ground-state configuration of the Fe_3As monolayer. IPDOS of *d* orbital for (b) Fe(I) and (c) Fe(II) atoms.

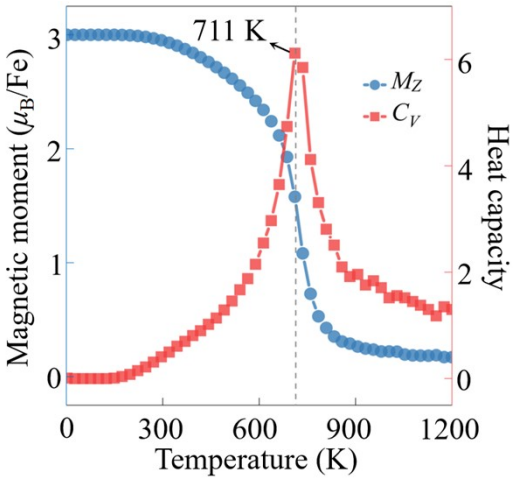

Fig. S7 The temperature-depended M_Z of each Fe ion and the C_V of the Fe_3As monolayer including J_1, J_2, and J_3.

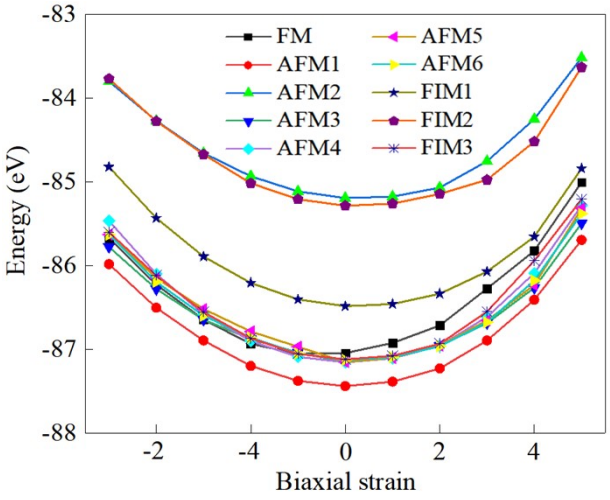

Fig. S8 Energies of each magnetic states of the Fe_3As monolayer from -5% to 5% biaxial strain.

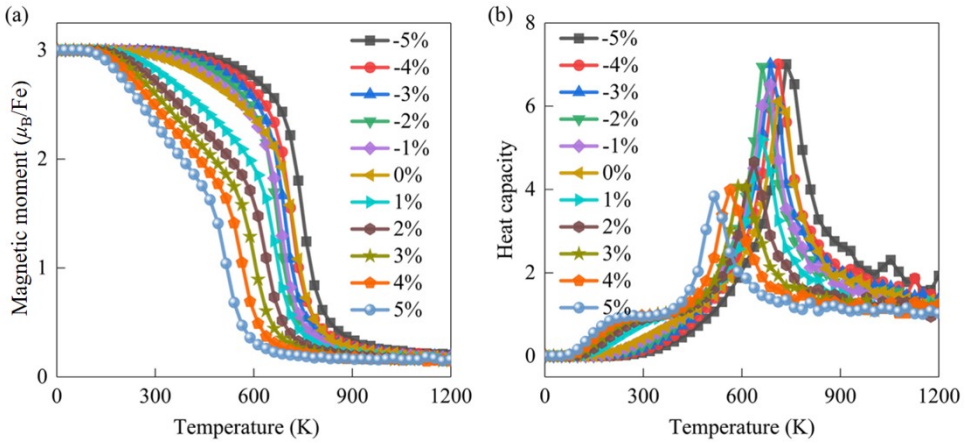

Fig. S9 The temperature-depended M_Z (a) and C_V (b) the Fe_3As monolayer under biaxial strain.

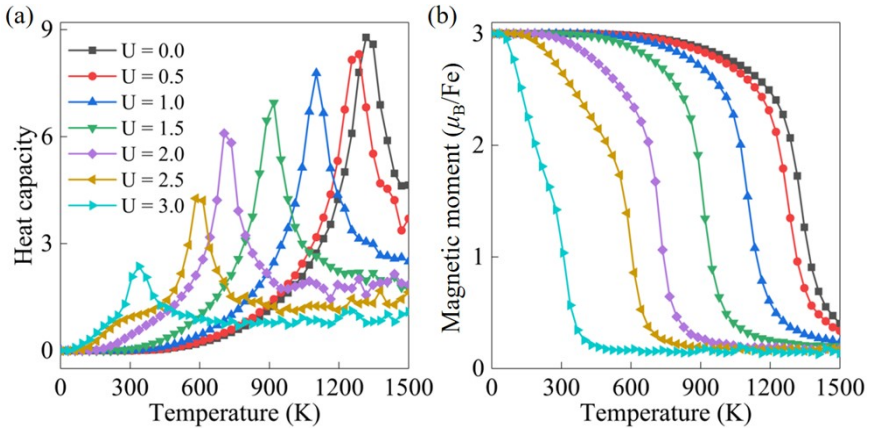

Fig. S10 The temperature-depended C_V (a) and M_Z (b) of the Fe_3As monolayer with the Hubbard on-site Coulomb potential (U) values from 0 to 3 eV.

Supplementary Tables

Table S1 Elastic constants (N/m) of the Fe_3As monolayer.

C_{11}	C_{12}/C_{21}	C_{22}	C_{66}
102.362	35.157	98.088	29.612

Table S2 The band gap (eV), magnetic moment (M in μ_B/Fe), exchange coupling parameters (Js in meV), and Néel temperature (T_N in K) of the Fe_3As monolayer under biaxial strain.

	Band-gap	$M_{Fe(I)}$	$M_{Fe(II)}$	J_1	J_2	J_3	T_N
-5%	0.09	2.85	2.83	87.79	10.49	-13.08	735
-4%	0.02	3.17	3.36	92.62	9.41	-13.598	711
-3%	1.20	3.46	3.27	96.40	8.81	-13.95	687
-2%	0.88	3.04	3.02	99.53	8.30	-14.01	662
-1%	0.84	3.11	3.50	101.75	7.28	-17.16	687
0	1.04	3.10	3.10	99.89	6.83	-21.01	711
1%	1.03	3.11	3.54	103.34	5.00	-24.38	662
2%	1.10	3.15	3.17	102.40	4.27	-25.96	638
3%	1.14	3.11	3.58	100.26	3.79	-26.14	589
4%	1.10	3.12	3.59	97.38	3.41	-25.51	564
5%	1.16	3.21	3.25	94.10	2.98	-24.32	515

Table S3 Structural information of the Fe_3As monolayer.

Phase	**Space Group**	**Lattice Parameters**	**Wyckoff Positions (fractional)**			
		(Å, °)	**Atoms**	***x***	***y***	***z***
Fe_3As	*Pmmm*	a = 4.1655	Fe(1*h*)	0.50000	0.50000	0.50000
		b = 4.6435	Fe(2*n*)	0.25978	0.50000	0.50000
		$\alpha = \beta = \gamma$ = 90.0000	As(1*d*)	0.50000	0.00000	0.50000

References

1 Y. Wang, J. Lv, L. Zhu and Y. Ma, *Comput. Phys. Commun.*, 2012, **183**, 2063-2070.

2 Y. Wang, J. Lv, L. Zhu and Y. Ma, *Phys. Rev. B*, 2010, **82**, 094116.

3 G. Kresse and J. Furthmüller, *Phys. Rev. B*, 1996, **54**, 11169.

4 E. Baerends, *Theor. Chim. Acta*, 2000, **103**, 265-269.

5 J. P. Perdew, K. Burke and M. Ernzerhof, *Phys. Rev. Lett.*, 1996, **77**, 3865.

6 K. Parlinski, Z. Q. Li and Y. Kawazoe, *Phys. Rev. Lett.*, 1997, **78**, 4063.

7 A. Togo, F. Oba and I. Tanaka, *Phys. Rev. B*, 2008, **78**, 134106.

8 G. Martyna, M. Klein and M. Tuckerman, *J. Chem. Phys.*, 1992, **97**, 2635-2643.

9 L. Liu, X. Ren, J. Xie, B. Cheng, W. Liu, T. An, H. Qin and J. Hu, *Appl. Surf. Sci.*, 2019, **480**, 300-307.

10 V. Wang, N. Xu, J.-C. Liu, G. Tang and W.-T. Geng, *Comput. Phys. Commun.*, 2021, **267**, 108033.

11 C. S. Liu, H. H. Zhu, X. J. Ye and X. H. Yan, *Nanoscale*, 2017, **9**, 5854-5858.

12 Y. Jiao, F. Ma, J. Bell, A. Bilic and A. Du, *Angew. Chem. Int. Ed.*, 2016, **55**, 1-5.

13 J. Wang, S. Yip, S. R. Phillpot and D. Wolf, *Phys. Rev. Lett.*, 1993, **71**, 4182-4185.